Postglacial paleoceanography of the western Barents Sea: implications for alkenone-based sea surface temperatures and primary productivity

Magdalena Łącka,[a,*] Min Cao,[b,c] Antoni Rosell-Melé,[c,d] Joanna Pawłowska,[a] Małgorzata Kucharska,[a] Matthias Forwick,[e] Marek Zajączkowski[a]

[a]Institute of Oceanology, Polish Academy of Sciences, Powstańców Warszawy 55, 81-712 Sopot, Poland

[b]Key Laboratory of Karst Environment, School of Geographical Sciences, Southwest University, Chongqing, 400715

[c]Institute of Environmental Science and Technology (ICTA-UAB), Universitat Autònoma de Barcelona, 08193 Bellaterra, Spain

[d]Institució Catalana de Recerca i Estudis Avançats, 08010 Barcelona, Spain

[e]Department of Geosciences, UiT The Arctic University of Norway in Tromsø, N-9037 Tromsø, Norway

*Corresponding author. E-mail address: mlacka@iopan.gda.pl

Keywords: alkenones, stratification, Holocene, sea ice decrease, global warming, North Atlantic Current, Arctic.

Highlights

- Postglacial SST and primary productivity in Storfjordrenna were reconstructed.
- Meltwater supply limited primary productivity during deglaciation.
- Mid-Holocene primary productivity was linked to both inhibited convective mixing and grazing.

- Late Holocene decrease in insolation facilitated brine production and nutrient resupply.

Abstract

The increasing influence of Atlantic Water (AW) in the Barents Sea, a process known as "Atlantification", is gradually decreasing sea ice cover in the region. Ongoing global climate warming is likely to be one of its drivers, but to further understand the role of natural variability and the biogeochemical impacts of the inflow of AW into the western Barents Sea, we reconstructed sea surface temperatures (SSTs) and primary productivity in Storfjordrenna, a climatically sensitive area south of Spitsbergen, between approximately 13,950 cal yr BP and 1300 cal yr BP. The alkenone $U^{K^*}_{37}$ proxy has been applied to reconstruct SSTs, and the alkenone accumulation rate in marine sediments has been used to infer changes in primary productivity. Our data show that the SST increase was concomitant with the progressive loss of sea ice cover and an increase in primary productivity in the western Barents Sea. We interpret these changes as reflecting the increasing influence of AW in the area as the ice sheets retreated in Svalbard. The transition from the Arctic to the Atlantic domain first occurred after 11,500 cal yr BP, as the Arctic Front moved eastward of the study site but with considerable variability in surface ocean conditions. High SSTs at approximately 6400 cal yr BP may have led to limited winter surface cooling, likely inhibiting convective mixing and the return of nutrients to the euphotic zone and/or enhanced organic matter consumption by zooplankton due to an earlier light signal in the ice-free Storfjordrenna. During the late Holocene (3600-1300 cal yr BP), low insolation facilitated sea ice formation and thus brine production. The former may have launched convective water mixing and increased nutrient resupply to the sea surface, consequently enhancing primary productivity in Storfjordrenna. We propose that, on the basis of the paleoceanographic evidence, the modern increasing inflow of warm AW and the disappearance

of pack ice on the Eurasian continental shelf are likely to weaken convective water mixing and decrease primary production in the region.

1. Introduction

The effects of ongoing climate warming are especially perceptible in the Arctic, mainly due to the rapid decline in the extent of sea ice over the past few decades, which numerous climate models expect to continue throughout the twenty-first century (e.g., Ding et al., 2017). The most striking changes in the extent and thickness of sea ice have occurred in the western Barents Sea (Onarheim et al., 2015; Yang et al., 2016). Sea ice decrease in the area is a reflection of the growing influence of Atlantic water (AW), a process sometimes referred to as "Atlantification" (e.g., Årthun et al., 2012; Oziel et al., 2016), which has caused the Barents Sea to reach its highest temperatures over the last decade, since systematic instrumental measurements began (Boitsov et al., 2012).

The accelerated loss of sea ice in the Barents Sea has a profound impact on the global energy budget, atmospheric and oceanic circulation, and the carbon cycle (Polyakov et al., 2017; Serreze and Barry, 2011). Among the Arctic shelf seas, the Barents Sea seafloor is the largest carbon sink, playing a significant role in controlling global atmospheric CO_2 concentrations and global climate (Smedsrud et al., 2013). Further decreases in ice cover and increases in surface water temperature in the western Barents Sea may cause primary productivity to decrease by 15-25% due to reduced nutrient flux into the upper ocean, resulting from decreasing advective mixing (Lewandowska et al., 2014; Lind et al., 2018). As the Barents Sea ecosystem supports some of the world's largest stocks of fish (Dalpadado et al., 2011 and references therein), this issue also has global economic importance. In addition, more organic matter could be buried, relatively speaking, in the seasonally ice-covered northern Arctic regions than in the ice-free areas of the western Barents Sea (Pathirana et al., 2014; Slagstad et al., 2011).

The "Atlantification" of the western Barents Sea is a process that has occurred in the recent geological past. After the Younger Dryas (YD), the inflow of AW to the western Barents Sea (Hald et al., 2007; Ślubowska-Woldengen et al., 2008) and maximum Holocene summer insolation (Berger and Loutre, 1991) caused the increase in sea surface temperatures (SSTs) and decrease in sea ice (Rasmussen et al., 2014). Sea ice-free conditions remained during most of the mid-Holocene as a result of the influence of AW (Łącka et al., 2015b). These conditions coincided with the highest Holocene primary productivity observed on the northern continental slope of the Barents Sea (Wollenburg et al., 2004).

The objective of this study is to reconstruct the impact of AW inflow to the western Barents Sea, and its influence on primary productivity, from c. 13,950 cal yr BP to c. 1300 cal yr BP. We based our reconstruction on the alkenone $U_{37}^{K^*}$ proxy to reconstruct SSTs (Bendle and Rosell-Melé, 2004) and the alkenone accumulation rate in marine sediments to infer the changes in primary productivity (e.g., Bolton et al., 2010). We compared our data to other studies conducted in the western Barents Sea continental slope (Martrat et al., 2003), the southwestern Barents Sea (Risebrobakken et al., 2010) and the Norwegian Sea (Calvo et al., 2002; Fig. 1; Table 1). The comparison provides new information on lateral and vertical oceanographic gradients, i.e., ocean vertical mixing, thermal stratification, and Arctic front movement in the western Barents Sea since the last deglaciation.

2. Oceanographic setting

The Barents Sea is an Arctic shelf sea located along the main pathway of heat and salt transport within the North Atlantic Current (NAC) entering the Arctic (Smedsrud et al., 2013; Rudels et al., 2015; Fig. 1). Thus, it is influenced by two main water masses, warm and saline AW and colder and fresher Arctic Water (ArW). AW (T>3°C, S>35.0; Loeng, 1991) is transported northwards by the NAC, following the continental slope of Norway (Fig. 1A). The topographically steered flow of NAC bifurcates into two branches c. 72°N (Fig. 1A). One

95 branch flows into the southern Barents Sea (i.e., North Cape Current), whereas the other branch
96 continues northwards along the western Barents Sea slope and western Svalbard margin into
97 the Arctic Ocean as the West Spitsbergen Current (Aagaard et al., 1987) (Fig. 1). The ArW
98 (T<0°C, S<34.4), formed by mixing of AW and polar waters in the Arctic Ocean, enters the
99 Barents Sea from the north and is carried southward by the East Spitsbergen Current (ESC)
100 (Loeng, 1991). At the boundary between Arctic and Atlantic water, a sharp gradient in terms of
101 temperature, salinity, and sea-ice distribution is formed called the Arctic Front (AF; Hopkins,
102 1991). The AF determines the position of the marginal ice zone and surface productivity in the
103 summer season (Smith and Sakshaug, 1990). At present, the AF is located east of our study
104 area; however, the frontal zone changes its position, and water mixes and exchanges across the
105 front (Walczowski, 2013; Łącka et al., 2015b).
106 The study area is the glacial trough of Storfjordrenna, located south of Spitsbergen (Fig.
107 1B). Storfjordrenna extends towards the north into Storfjorden, which is located north of a sill
108 of 120 m depth. AW flows into Storfjordrenna in a cyclonic manner parallel to the trough's
109 southern margin and along the northern slope towards its mouth (Fer et al., 2003). ArW enters
110 the trough from the southeast with the ESC (Loeng, 1991). The uppermost 500 m of the water
111 column at the mouth of Storfjordrenna contains relatively warm (4–7°C) and saline (35.2) AW
112 (Fig. 2A). Cold (−0.5°C) intermediate water, generated by convection in the Nordic seas, occurs
113 beneath the AW (Nilsen et al., 2008).
114 In the central part of Storfjordrenna, AW occurs between 50 and 160-m water depth (Fig.
115 2B). However, it is cooler here (max. 4.2°C) than in the outer part of the Spitsbergen shelf (Fig.
116 2A). The surface water (SW) reaches 3.8°C, which is comparable to the temperature of the AW
117 at the Storfjordrenna mouth. However, it has a lower salinity (33.5; Fig. 2B) than the AW at the
118 Storfjordrenna mouth. During the winter-freezing period, which typically lasts from late
119 November to mid-May, brine-enriched shelf water (BSW) is produced in Storfjorden

(Haarpaintner et al., 2001; Skogseth et al., 2004). BSW fills Storfjorden to the top of the sill and then begins a gravity-driven overflow through Storfjordrenna, further down the continental slope (Schauer et al., 2003). Thus, in Storfjordrenna, a 30-m-thick layer of BSW (temperature of approximately 0°C and salinity slightly over 35.1) usually occurs in the deepest region immediately above the seafloor (Fig. 2B).

Northeast from Storfjordrenna, in the northern Barents Sea, AW flows via the Franz-Victoria Trough and the Kvitøya Trough, from the Eurasian continental slope (Fig. 1; Pfirman et al., 1994; Lind and Ingvaldsen, 2012) below the sea surface dominated by ArW (Gammelsrød et al., 2009). ArW occupies the upper 20–100 m of the northern Barents Sea, with temperature down to the freezing point (Lind and Ingvaldsen, 2012), whereas AW is found at depths of 150–350 m, has a salinity of 34.7 and a temperature of 1.1–0.8°C (Fig. 2C) (Klitgaard-Kristensen et al., 2013). The northern Barents Sea experiences seasonal sea ice cover that forms during fall/winter (Loeng, 1991). Sea ice breakup occurs during summer, leading to open-water conditions in August and September (Belt et al., 2015). Recently, there is observed a decline in sea-ice formation in the northern Barents Sea, due to decrease in sea-ice import through the passage between Franz Josef Land and Novaya Zemlya, and a corresponding loss in freshwater, leading to weakened ocean stratification, enhanced vertical mixing and increased upward fluxes of heat and salt (Lind et al., 2018).

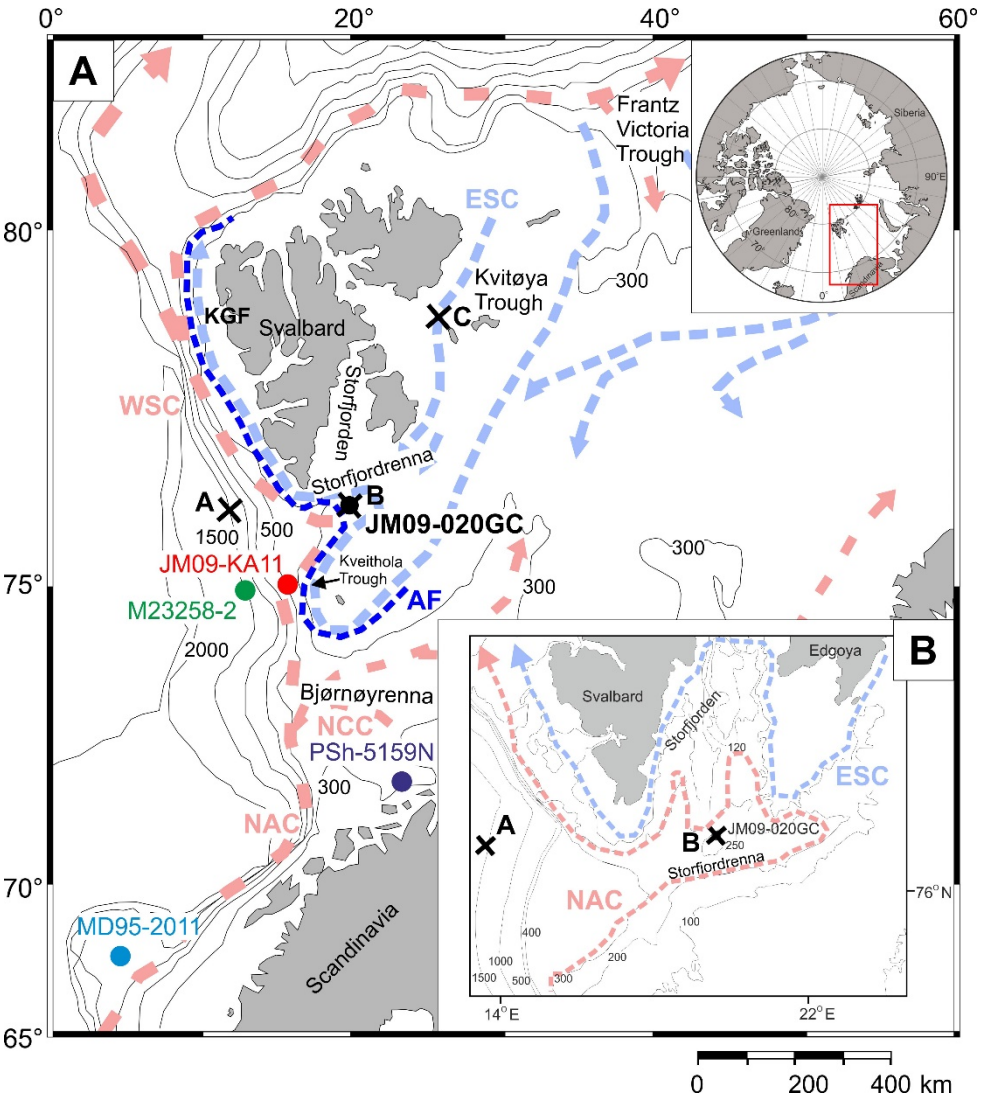

Fig. 1. Simplified map showing place names and core locations mentioned in the text, the dominant present-day surface water circulation in the Nordic and Barents Seas. The location of the studied core JM09-020 and the locations of the cores discussed in this paper are marked with dots: MD95-2011 (Calvo et al., 2002), PSh-5159N (Risebrobakken et al., 2010), M23258-2 (Martrat et al., 2003), and JM09-KA11 (Belt et al., 2015). Conductivity-temperature-depth (CTD) stations (A, B, and C) are marked with a black X. Red arrows represent Atlantic Water (AW), blue arrows represent Arctic Water (ArW), and royal blue dashed lines represent the Arctic Front (AF). The remaining abbreviations are as follows: NAC - North Atlantic Current, NCC- North Cape Current, WSC - West Spitsbergen Current, and ESC - East Spitsbergen Current.

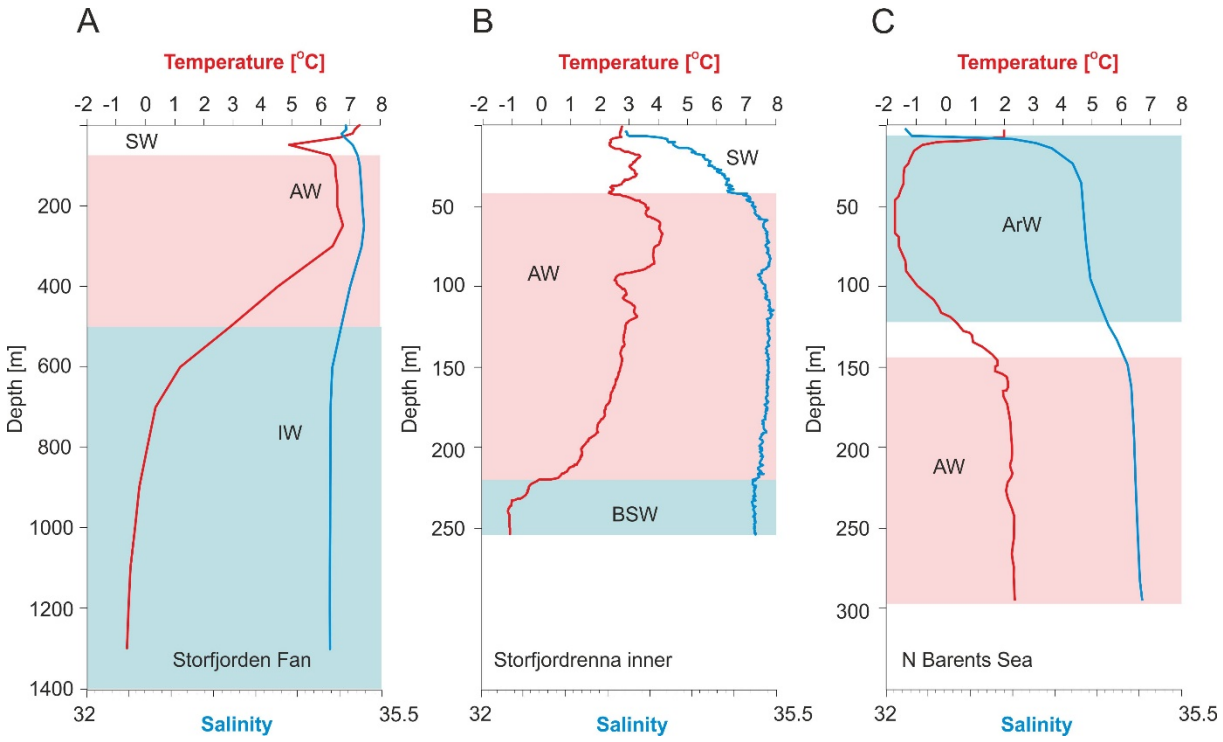

Fig. 2. Temperature and salinity profiles from A) the continental slope at the mouth of Storfjordrenna measured in August 2012 (1300-m water depth) (selected from the World Ocean Database https://www.nodc.noaa.gov/OC5/SELECT/dbsearch/dbsearch.html); B) Storfjordrenna (JM09-020GC) measured in August 2015 at the inner part of the trough (253-m water depth; this study); C) the Kvitøya Trough (NP05-49) measured in August 2005 (300-m water depth) (Klitgaard-Kristensen et al., 2013). The colors on the conductivity-temperature-depth (CTD) profiles indicate the prevailing water masses. Abbreviations: SW - surface water, AW - Atlantic Water, ArW- Arctic Water, IW - intermediate water, and BSW - brine-enriched shelf water. The locations of the CTD stations are indicated in Fig. 1.

3. Materials and methods

3.1. Sediment cores

A 4.25-m-long gravity core JM09-020-GC (76.31489° N, 19.69957° E) was retrieved from a 253-m water depth in Storfjordrenna, with the R/V Jan Mayen (now: Helmer Hanssen; UiT

164 The Arctic University of Norway) in November 2009 (Fig. 1). The coring site is located inside
165 Storfjordrenna in a 3-km broad flat plain (<1% inclination); its location was selected after an
166 echo-acoustic investigation in an area whose sediments were not under direct influence of brine-
167 enriched waters. Conductivity-temperature-depth (CTD) measurements were performed in
168 August 2015 at the coring site (Fig. 1 and Fig. 2).

169 The new results from core JM09-020-GC were compared to previously published alkenone
170 data (Table 1). Core PSh-5159N (Risebrobakken et al., 2010) was retrieved from the SW
171 Barents Sea (Fig. 1) at a water depth of 422 m. Its basal age is c. 15,000 cal yr BP. Core
172 M23258-2 (Martrat et al., 2003) was recovered from the Barents Sea continental slope (Fig. 1)
173 at a depth of 1768 m, and it spans over 15,000 cal yr BP. Core MD 95-2011 was collected in
174 the eastern Norwegian Sea at a water depth of 1048 m (Fig. 1) and was dated to c. 13,800 cal
175 yr BP (Calvo et al., 2002).

176

177 **Table 1**

178 Positions of the cores and references to the original publications discussed in this paper.

Core	Location	Reference	Latitude (N)	Longitude (E)	Water depth (m)
JM09-020-GC	Storfjordrenna	This study	76.31°	19.70°	253
MD95-2011	NE Norwegian Sea	Calvo et al. (2002)	66.97°	7.63°	1048
PSh-5159N	SW Barents Sea	Risebrobakken et al. (2010)	71.36°	22.65°	422
M23258	W Barents Sea	Martrat et al. (2003)	74.99°	13.97°	1768

3.2. Chronology

A lithological description and a chronology of core JM09-020-GC were published by Łącka et al. (2015b). The AMS ^{14}C dates were converted into calibrated ages using the Marine13 calibration curve (Reimer et al., 2013) and a ΔR 105±24 (Mangerud et al., 2006) in the calibration program Calib 7.1 (Stuiver and Reimer, 1993). The basal age of the sediment core was 13,950 cal yr BP. The lithological and micropaleontological investigation of the sediment core revealed that the core apparently represents continuous sedimentation, with no signs of redeposition and/or lateral sediment transport. The uppermost c. 40 cm of sediments were lost during coring; therefore, the age model for the sediment surface is cut off at 1300 cal yr BP (Łącka et al., 2015b). The time resolution of the record was between 10 and 400 years, depending on the core depth with the lowest resolution identified during the mid-Holocene (Supplement 1). The previously published age models for cores MD95-2011, PSh-5159N and M23258 have been recalibrated using Marine13 radiocarbon calibration curve (Reimer et al., 2013) in Calib 7.1 (Stuiver and Reimer, 1993).

3.3. Alkenone analysis

The alkenone analysis methodology is consistent with the standard methodology developed by Bendle and Rosell-Melé (2004). Individual subsamples for biomarker analysis collected at 1-5 cm intervals were ultrasonically extracted with dichloromethane/methanol (DCM/MeOH 3:1, v/v). An internal standard (2-nonadecanone, $C_{19}H_{38}O$, 3.5 ng/μL) was added to each test tube prior to the extraction of the biomarkers. The samples were extracted three more times using the same procedure, combined and treated with acid-activated copper to remove elemental sulfur. The total extracts were cleaned with open-column chromatography using hexane:DCM (1:1, v/v; 6 mL) and 6 mL of DCM (alkenone fraction).

Long-chain alkenones were quantified on an Agilent 7890A gas chromatograph with a flame ionization detector (GC-FID). The compounds were eluted through an Agilent HP-1

capillary column with a length of 60 m, an internal diameter of 0.25 mm, and a film thickness of 0.25 μm. External standards were used to identify the alkenones in the GC-FID based on their retention time. The quantification of alkenones was assessed using known concentrations of internal standards added prior to extraction. A solvent blank and sediment standard from Fram Strait (Rueda, 2013) were extracted with each batch of samples and analyzed in the same way as the rest of the samples. This routine allowed for the control of possible contamination during the preparative analysis of the samples and helped to recognize the alkenone peaks.

Alkenones are used widely to calculate the U_{37}^{K} indices in the North Atlantic region (Łącka et al., 2015a and references therein). The degree of alkenone unsaturation (the number of double bonds between the carbon atoms) provides an established way to reconstruct past ocean conditions (Brassell et al., 1986; Herbert, 2001; Marlowe et al., 1984; Volkman et al., 1980). However, according to Rosell-Melé (1998), when the $\%C_{37:4}$ value constitutes more than 5% of the total $\%C_{37}$ alkenone value and U_{37}^{K} is negative, the calculated temperatures are unreliable. In the case of JM09020-GC, the values generally exceeded 5%. An alternative index to estimate SSTs for samples when $C_{37:4}$ values are significantly high was proposed by Bendle and Rosell-Melé (2004) as follows:

$$U_{37}^{K^*} = \frac{C_{37:2}}{C_{37:2} + C_{37:3} + C_{37:4}}$$

SSTs can be reconstructed using the alkenone-derived $U_{37}^{K^*}$ index (Bendle and Rosell-Melé, 2004) according to the following equation by Müller et al. (1998):

$$T(°C) = \frac{U_{37}^{K^*} - 0.044}{0.033}$$

The statistical error of the regression is 1.5°C. According to Müller et al. (1998) and Conte et al. (2006), the global core-top calibration of alkenone-based SST revealed that the best fit is obtained with annual mean SSTs. The same relationship was also established for polar and

frontal regions (e.g., Müller and Fisher, 2003). In the study area, alkenone producers can bloom in summer, as well as in autumn when stratification of the upper water column breaks down, i.e., the sedimentary signal would potentially integrate a wider range of temperatures than just those from the warmest season.

To facilitate the comparison of our results with the published alkenone SST records in Calvo et al. (2002) and Martrat et al. (2003), we have recalculated the U^{K}_{37}-based SSTs according to the Bendle and Rosell-Melé (2004) U^{K*}_{37} model. The SST data after Risebrobakken et al. (2010) are presented in the original form, as the raw data are unavailable.

The total abundance of $C_{37:4}$ alkenones in the record was used as a tracer to infer variations in the water mass type as follows (Bendle et al., 2005):

$$\%C_{37:4} = \frac{C_{37:4}}{C_{37:2} + C_{37:3} + C_{37:4}} x100$$

In the subpolar and polar regions of the Nordic Seas, there is an increased proportion of the $C_{37:4}$ alkenone relative to the $C_{37:3}$ and $C_{37:2}$ alkenones (Rosell-Melé et al., 1994, Rosell-Melé 1998). High $\%C_{37:4}$ values are associated with ArW, whereas low values are related to AW (Bendle et al., 2005). Hence, $\%C_{37:4}$ can also be used as an indicator of the AF position in the Nordic Seas (Rosell-Melé et al., 1998)

The absolute quantification of alkenones ($C_{37:2} + C_{37:3} + C_{37:4}$) was assessed using known concentrations of internal standards added prior to extraction and expressed as $\square C_{37}$ ng g^{-1} of dry sediment. The estimated level of detection was 3 ng g^{-1}, using an average sediment sample of 1 g dry weight. Concentration versus depth profiles can be potentially misleading with respect to quantitative interpretation of alkenone data, since they do not adequately reflect the influences of any changes in bulk sediment properties or accumulation rates. Therefore, alkenone concentrations were converted to annual fluxes, by combining individual sediment

concentrations with sediment densities and accumulation rates derived from dry bulk density data and age/depth models, respectively.

4. Results

The SSTs in the lowermost part of the core (13,950-12,800 cal yr BP) varied between 0.5°C and 5.5°C (Fig. 3B). Both the alkenone flux and concentration (C_{37}) were low (0.3-1.4 ng cm^{-2} a^{-1} and 7-32 ng g^{-1} sed, respectively; Fig. 3D), with a high contribution of $C_{37:4}$ (between 13% and 79%; Fig. 3A).

At approximately 12,800 cal yr BP, the alkenone concentrations dropped below the detection limit (Fig. 3D). Thus, SST estimates are missing. At approximately 12,600 cal yr BP, Storfjordrenna was covered by cold (T<1°C) surface water (Fig. 3B) with a high contribution of $C_{37:4}$ (c. 58%). Between 12,500 cal yr BP and 11,700 cal yr BP, the SSTs were slightly higher (average 2°C; Fig. 3B), and the alkenone flux remained low (average 0.3 ng cm^{-2} a^{-1}; Fig. 3D). After 11,700 cal yr BP, the alkenone flux increased (up to 4 ng cm^{-2} a^{-1}; Fig. 3D) with a simultaneous decrease in $\%C_{37:4}$ (Fig. 3A).

A distinct decrease in $\%C_{37:4}$ (from 50% to approximately 25%; Fig. 3A) occurred c. 11,500 cal yr BP. This decrease was followed by a substantial SST increase, from an average of 2°C to an average of 8.4°C; however, SST oscillated significantly from 3°C to 12.5°C (Fig. 3B). At the same time, the alkenone flux remained relatively high (average 1.6 ng cm^{-2} a^{-1}; Fig. 3D).

Between 9200 cal yr BP and 3400 cal yr BP, SSTs in Storfjordrenna remained highly variable (from 3°C to almost 13°C; Fig. 3B). The $\%C_{37:4}$ varied between 7% and 38% (Fig. 3A), and the alkenone flux was very low (between 0.08 and 0.61 ng cm^{-2} a^{-1}).

After 3400 cal yr BP, the SSTs in Storfjordrenna ranged between 0.2°C and 10°C (Fig. 3B), with a rapid, concomitant increase in the alkenone flux (from 0.5 to 3 ng cm^{-2} a^{-1}). Towards the

upper part of the core, the alkenone flux increased even more, reaching 12 ng cm^{-2} a^{-1} c. 1500 cal yr BP (Fig. 3D). At the same time, the $\%C_{37:4}$ varied between 9% and 25%; Fig. 3A).

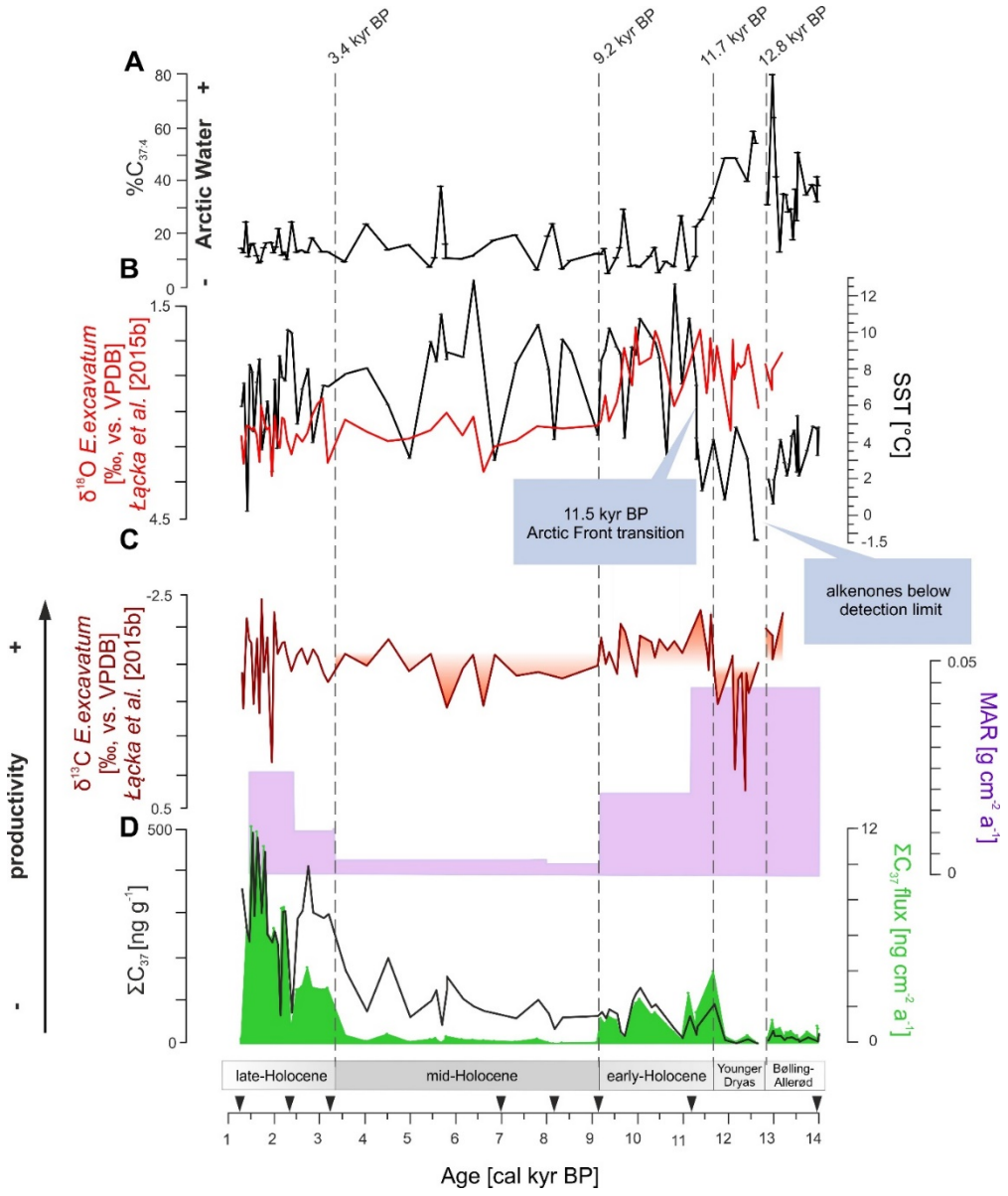

Fig. 3. Proxy records from core JM09-020GC A) $\%C_{37:4}$; B) $U^{K}_{37}{}^{*}$-based sea surface temperatures (SSTs; right scale) and stable oxygen isotope data (red line; left scale; Łącka et al., 2015b); C) stable carbon isotope data (burgundy line; left scale; Łącka et al, 2015b) and mass accumulation rates (g cm^{-2} a^{-1}; violet shading; right scale; Łącka et al., 2015b); D) total alkenone concentrations (□C37; ng g^{-1}; black line; left scale) and total alkenone flux (ng cm^{-2} a^{-1}; green shading; right scale). The black triangles on the x axis denote the AMS ^{14}C converted

to calibrated radiocarbon ages (after Łącka et al., 2015b). The Arctic Front transition at 11,500 cal yr BP is marked.

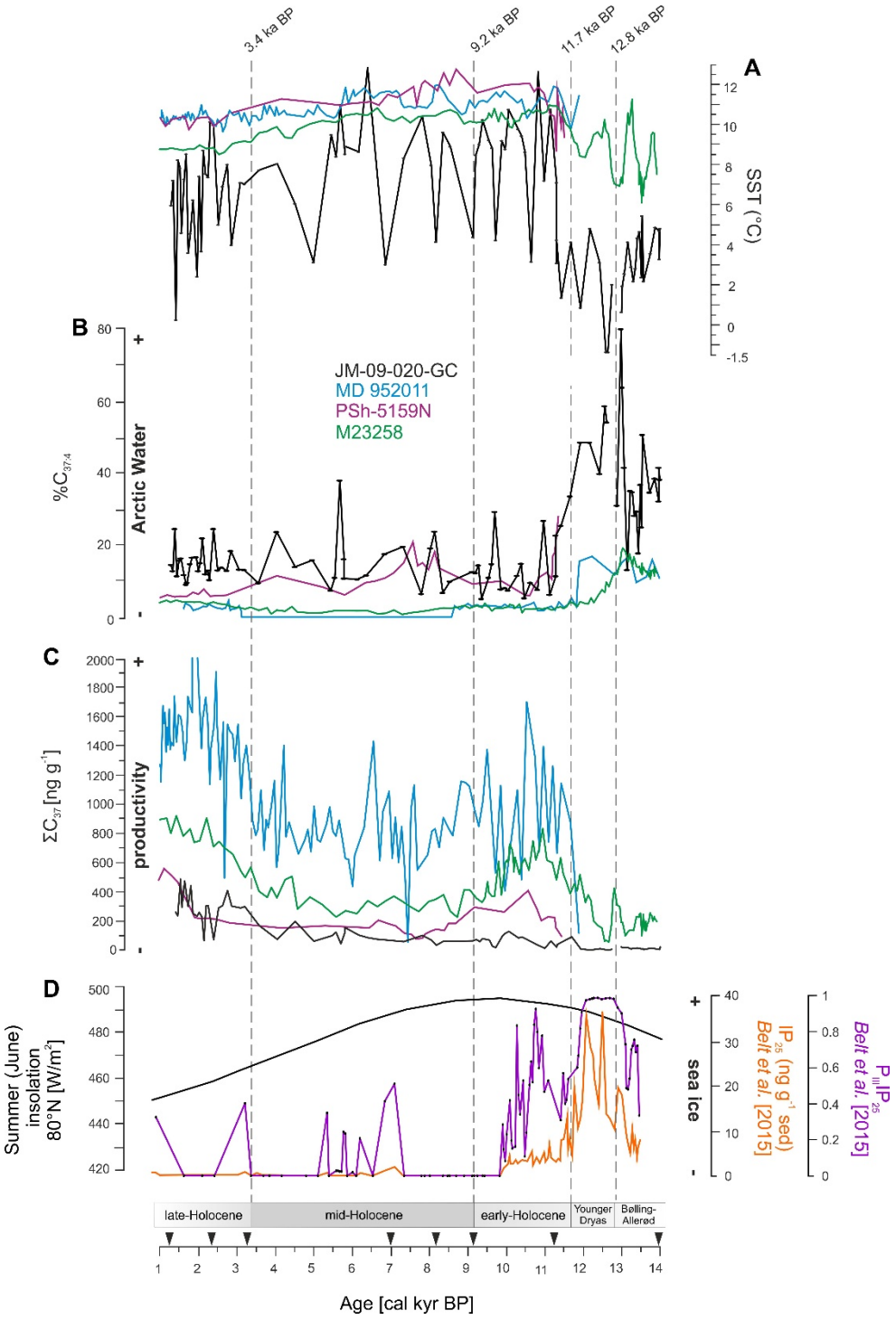

Fig. 4. Comparison of A) $U^{K}_{37}*$-based sea surface temperatures (SSTs; right scale); B) $\%C_{37:4}$; C) total alkenone concentrations (□C37; ng g^{-1}) from the current study (JM09-020GC; black line), western Barents Sea (Martrat et al., 2003) (M23258; green line), the southwestern Barents

289 Sea (Risebrobakken et al., 2010) (PSh-5159N; purple line), and the northeastern Norwegian
290 Sea (Calvo et al., 2002) (MD95-2011; blue line); and D) summer insolation (June) at 80°N
291 (Berger and Loutre, 1991; black line, left scale) and IP_{25} (orange line, right scale), and $P_{III}IP_{25}$
292 (purple line, right scale) records from the core JM09-KA11 obtained from the western Barents
293 Sea (after Belt et al., 2015) showing the sea ice conditions. The black triangles on the x axis
294 denote the AMS ^{14}C converted to calibrated radiocarbon ages (after Łącka et al., 2015b).

295 **5. Discussion**

296 **5.1. Bølling-Allerød (13,950-12,800 cal yr BP)**

297 Grounded ice retreated from Storfjordrenna during the B-A warming, c. 13,950 cal yr BP
298 (Łącka et al., 2015b), as a consequence of the overall warming caused by the increase in the
299 northern hemisphere insolation (Berger and Loutre, 1991). The SSTs at the study site during
300 the B-A varied between 2°C and 4°C (Fig. 3B), which is comparable to modern SST values in
301 Storfjordrenna (Fig. 2B). The modern-like conditions have also been noted on the Barents Sea
302 continental slope, where SST reached 11°C during the B-A (Martrat et al., 2003; Fig. 4A),
303 which is comparable to the modern summer SST in this region (Trudnowska et al., 2016).
304 Furthermore, the low $P_{III}IP_{25}$ (sea ice proxy) in the Kveithola Trough, south of Storfjordrenna
305 (see the location of the JM09-KA11 core in Fig. 1), indicate stable ice edge or marginal ice
306 zone conditions at that time (Fig. 4D) (Belt et al., 2015). The sea ice conditions in
307 Storfjordrenna during the B-A could be driven by prevailing southwesterly winds. The modern
308 sea ice occurrence in Storfjordrenna arises from seasonal ice advected from the Arctic Ocean
309 and the Barents Sea (Hendricks et al., 2011) and is strictly connected to the prevailing wind
310 direction. According to Skogseth et al. (2004), the amount of sea ice in the western Barents Sea
311 is high during winters dominated by northeasterly winds and when temperatures are low,

whereas in winters dominated by southwesterly winds, the inflow of the AW increases SSTs, and the sea ice decreases.

Although the B-A SSTs were comparable to contemporary values, the alkenone concentration and flux at the study site were low (Fig. 3D), with a high contribution of $C_{37:4}$ (between 13% and 79%; Fig. 3A). This inverse relationship between C_{37} and $C_{37:4}$ indicates that fewer alkenones were produced in the fresher ArW. High $\%C_{37:4}$ values have been found in modern surface sediments in regions where surface temperatures and salinity are both low (Bendle and Rosell-Melè, 2004; Bendle et al., 2005; Harada et al., 2006), e.g., high $\%C_{37:4}$ values (up to 70%) have been noted in the waters of the East Greenland Current, where the sea ice cover reached approximately 80% (Bendle et al., 2005). Phytoplankton productivity is much lower in these ArWs than in AWs (Andreassen et al., 1996). However, the low concentration of alkenones could also result from their degradation and/or dilution by the high sediment supply (e.g., Hoefs et al., 1998). A high sediment accumulation rate in Storfjordrenna (43 g $cm^{-2}kyr^{-1}$) during this interval (Fig. 3C; Łącka et al., 2015b) supports the latter interpretation.

Much lower alkenone concentrations during the B-A were also noted on the Barents Sea continental slope (Martrat et al., 2003), indicating that the AF was located further to the west than it is today. This difference was caused by the proximity of the retreating Svalbard Barents Sea Ice Sheet (SBSIS) front, which was located in the inner basin of Storfjorden at that time (e.g., Rasmussen and Thomsen, 2014) and released large amounts of turbid meltwater (Łącka et al., 2015b), limiting primary productivity (Fig. 4C). This process is observed today in glaciated fjords on Svalbard, where, despite relatively high SSTs, productivity remains low (Kubiszyn et al., 2014; Piwosz et al., 2009; Zajączkowski, 2008). We conclude that the oceanographic conditions in Storfjordrenna during the B-A were similar to modern conditions in the innermost parts of the glaciated fjords of western Svalbard.

5.2. Younger Dryas (12,800-11,700 cal yr BP)

The onset of the YD (12,800 cal yr BP) in Storfjordrenna was characterized by low alkenone concentrations, occasionally remaining below the detection limit (Fig. 3D). This extremely low alkenone signal indicates a reduction in primary productivity that persisted for several decades. Similarly, low or absent primary production is observed beneath modern pack ice in the Arctic Ocean (Antoniades et al., 2011; Darby et al., 2006), suggesting that sea ice covered the area. Another explanation for the low or lack of alkenone signal might be postdepositional degradation. However, Łącka et al. (2015b) noticed, based on the absence of ice-rafted debris in this interval, that the beginning of YD in Storfjordrenna was characterized by temporary polar conditions and the formation of perennial pack ice in Storfjorden that locked icebergs proximal to their calving fronts, thus preventing their movement over the coring site. Therefore, we suggest that Storfjordrenna was covered by perennial sea ice at the onset of the YD, limiting light penetration into the surface water and subsequently restricting phytoplankton growth.

At c. 12,600 cal yr BP, Storfjordrenna was covered by cold (T<1°C) surface water (Fig. 3B) of Arctic origin, as seen from the high values of $\%C_{37:4}$ (Fig. 3A). The surface productivity at the study site increased slightly (Fig. 3D). However, Łącka et al. (2015b) noted a lighter $\delta^{18}O$ signal from benthic foraminifera, indicating the presence of warmer waters at the bottom (Fig. 3B). The nearly continuous presence of warmer and more saline AW during the beginning of the YD was also noted in the subsurface waters of the southern Nordic Seas by Knudsen et al. (2004) and Rasmussen et al. (2011). The difference between cold, less saline surface water and warmer but high saline bottom water indicates stratification, which was essential for the presence of sea ice, since the pycnocline protected the cold sea surface from the heat stored in the AW below. According to Rasmussen et al. (2014), the pycnocline over the western Spitsbergen shelf occurred at depths between 100 m and 150 m at this time, because of the freshwater supply from the decaying SBSIS. Our data may indicate that the oceanographic

conditions of Storfjordrenna at this time were similar to modern conditions in the northern Barents Sea (Fig. 1), with strong water column stratification, prolonged seasonal sea ice cover (Fig. 2C) and lower marine productivity (Fig. 3D). However, as the lighter $\delta^{18}O$ can also point to the changes in bottom water salinity, more studies are needed to confirm our hypothesis. Nevertheless, the severe seasonal sea ice cover throughout the YD also occurred 150 km south of our coring site, in the Kveithola Trough, as indicated by high $P_{III}IP_{25}$ values (Belt et al., 2015) (Fig. 4D). Further west, the continental margin remained ice free; however, the SST decreased to 7°C, and the alkenone production also decreased significantly (Martrat et al., 2003; Fig. 4C).

Between 12,500 cal yr BP and 11,700 cal yr BP, the SST in Storfjordrenna increased (average 2°C); however, surface productivity remained low (Fig. 3B and Fig. 3D). This might have resulted from the continuous delivery of turbid waters from the decaying SBSIS (Łącka et al., 2015b), which strongly limited light penetration and consequently led to decreased primary productivity and/or alkenone signal dilution (compare with Hoefs et al., 1998). At the same time, the mineral particles in the surface waters absorbed an amount of sunlight energy (e.g., Kara et al., 2004) that was close to the maximum Holocene values (Fig. 4D), thereby elevating the SST in Storfjordrenna. A widespread hypothesis regarding the mechanism of the YD cold spell suggests that the YD cooling resulted from a slowdown in the AMOC (e.g., Ritz et al. (2013) and references therein). Nevertheless, AW influenced numerous locations in the North Atlantic region throughout the YD (Bartels et al., 2017; Łącka et al., 2015b; Pearce et al., 2013; Rasmussen et al., 2007), leading to variable sea ice conditions in the Nordic Seas during the latter part of YD (Bakke et al., 2009; Cabedo-Sanz et al., 2013). Our data indicate that heavy sea ice conditions prevailed in Storfjordrenna only at the very beginning of the YD. In the later part of YD, the oceanography of Storfjordrenna was modified by interactions between Arctic and Atlantic waters, as indicated by the variability in SST (Fig. 3B) and $\%C_{37:4}$ (Fig. 3A). The similar pattern in alkenone record has been also observed on the continental

386 slope of the Barents Sea, where after 12,200 cal yr BP ArW contribution decreased concomitant
387 with the productivity increase (Fig. 4 B and C). Contradictory, the $P_{III}IP_{25}$ signal from Kveithola
388 Trough pointed to the continuous presence of consistently long seasonal sea ice cover (Belt et
389 al., 2015).

390 **5.3. Early Holocene (11,700-9200 cal yr BP)**

391 At the beginning of the early Holocene (11,700 cal yr BP), the alkenone concentrations in
392 Storfjordrenna increased and the $\%C_{37:4}$ decreased, indicating the increasing influence of AW
393 in the trough, a reduction in sea ice, as well as an increase in marine productivity (Fig. 3C). A
394 similar oceanographic change was noted in the southwestern Barents Sea by Risebrobakken et
395 al. (2010) and in the Norwegian Sea by Calvo et al. (2002). In the record after Martrat et al.
396 (2003), further decrease in $\%C_{37:4}$ and increase in productivity was observed. The transition
397 from prolonged seasonal ice cover to ice-edge conditions is also supported by the $P_{III}IP_{25}$ signal
398 from the western Barents Sea, which indicates that sea ice cover at that time was variable (Belt
399 et al., 2015).

400 Approximately 11,500 cal yr BP, a rapid transition from an Arctic to an Atlantic water-
401 dominated environment occurred in Storfjordrenna, suggesting that AF passed our study site
402 and moved eastward. This is illustrated by a further decrease in $\%C_{37:4}$ (from 50% to
403 approximately 25%; Fig. 3A) and a substantial SST increase, from an average of 2°C prevailing
404 during the YD to 3-12.5°C at the beginning of the Holocene (Fig. 3B). Today, such high SSTs
405 (average 8.4°C; Fig. 3B) are observed in the core of the West Spitsbergen Current flowing west
406 of Spitsbergen (e.g., Trudnowska et al., 2016); however, they are less variable than the SSTs
407 during the early Holocene. A significant increase of SSTs shows AW appearance in the upper
408 part of the water column. However, the high amplitudes in SST prevailing throughout the entire
409 Holocene indicate the continuous proximity of the AF to our study site (Fig. 3B). The SST

variability presented in Fig. 3B corresponds to the pulsatory inflow of ArW shown in Fig. 3A. The location of the AF closer to the Spitsbergen coast at approximately 11,500 cal yr BP is also confirmed by the increase in productivity in Storfjordrenna (higher alkenone flux and lighter $\delta^{13}C$; Fig. 3C and D). The presence of a highly productive frontal zone at our study site is also visible in the higher abundance of the AF proximity proxy, i.e., the benthic foraminifera *Nonionellina labradorica,* in Storfjordrenna (Łącka et al., 2015b). The timing of the AF transition in Storfjordrenna was the same as that on the Barents Sea continental slope (Martrat et al., 2003) and that farther south in the eastern Norwegian Sea (Calvo et al., 2002) (Fig. 4B), where $\%C_{37:4}$ decreased to modern values characteristic of the AW domain, i.e., 5% (Rosell-Melé et al., 1998). Previously, Łącka et al. (2015b) based on $\delta^{18}O$ concluded that the transition from the Arctic to the Atlantic domain occurred at approximately 9600 cal yr BP (Fig. 3B), because the lighter $\delta^{18}O$ is characterized for the ArW of Barents Sea origin (Duplessy et al., 2005). Indeed, the $\delta^{18}O$ values are still shifted towards the lighter values, but this could be also caused by the continuous production of brine in Storfjordrenna. Although the AW dominated at the surface, sea ice formed during the polar night, and lower $\delta^{18}O$ brine was delivered to the bottom of Storfjordrenna (Fig. 3B).

Early Holocene SSTs in Storfjordrenna were variable and reached the Holocene temperature maximum (Fig. 3B). Because the alkenone record is susceptible to temperature changes related to orbital forcing (Risebrobakken et al., 2011), we suggest that the SST changes observed during the early Holocene in Storfjordrenna and on the adjacent continental shelf resulted from both AW inflow and a peak in the northern hemisphere summer insolation (Berger and Loutre, 1991) (Fig. 4D). The presence of warm AW was found in the early Holocene at the northern tip of Svalbard (Bartels et al., 2017) and even farther in the northwestern Barents Sea (Ivanova et al., 2019). The appearance of AW at the sea surface in Storfjordrenna suggests that the contribution of turbid meltwater diminished, as confirmed by the reduced sediment

accumulation rate at the core site during the early Holocene (Fig. 3C; Łącka et al., 2015b). Indeed, according to Forwick and Vorren (2009) and Hughes et al. (2016), after the YD-early Holocene transition, the final deglaciation of Svalbard and Scandinavia occurred, and after 10,000 cal yr BP, the glaciers in western Svalbard were even smaller than those of the present day.

5.4. Mid-Holocene (9200-3400 cal yr BP)

SSTs in Storfjordrenna varied significantly during the mid-Holocene (Fig. 3B), although in the western Barents Sea continental margin (Martrat et al., 2003) and in the Norwegian Sea (Calvo et al., 2002) they remained stable (10°C and 11.5°C, respectively) (Fig. 4A). Over the European continental slope, warm AW dominated at the surface during this period, as confirmed by the absence or low values of $C_{37:4}$ alkenone (Fig. 4B; Calvo et al., 2002; Martrat et al. 2003). Conversely, high $\%C_{37:4}$ (10-20%) values were found in Storfjordrenna sediments (Fig. 3A; this study) and in the southwestern Barents Sea (Risebrobakken et al., 2010), which could suggest a continuous ArW contribution (Fig. 4B) at those sites. A feasible explanation of the SST variability on the western shelf of the Barents Sea could be the alternating influence of the ESC with the NAC.

At approximately 6400 cal yr BP, the SST in Storfjordrenna reached a peak of almost 13°C (Fig. 3B) and the $\%C_{37:4}$ decreased (Fig. 3A), indicating significant AW inflow. Based on benthic foraminifera assemblages, especially the occurrence of *Melonis barleeanum*, Łącka et al. (2015b) suggested that around that time, the Storfjordrenna sea environment was similar to that of the contemporary Norwegian fjords, which are dominated by AW with temperatures of 6-8°C. Our new alkenone data confirm this finding. Additionally, the finding is supported by the occurrence of *Mytilus edulis* on the western and eastern coasts of Svalbard at this time (Salvigsen, 2002; Mangerud and Svendsen, 2017), as *M. edulis* is a thermophilous mollusk

spawning at temperatures above 8-10°C (Thorarinsdóttir and Gunnarsson, 2003). The mid-Holocene is often referred to as the Holocene Thermal Maximum (HTM) in marine and terrestrial records (Risebrobakken et al., 2011). The high SST predominated throughout the European Arctic, reducing sea ice formation up to the northern margins of the Svalbard shelf (Müller et al., 2012) and in the central Arctic Ocean (Polyak et al., 2010). However, the SST maximum occurred when the summer insolation had already started to decrease, after a maximum peak during the early Holocene (Berger and Loutre, 1991; Fig. 4D). This indicates that, at this time, the main heat source was the enhanced inflow of AW, and insolation played a secondary role in the heating of Storfjordrenna surface waters.

During the mid-Holocene, the alkenone flux in Storfjordrenna was very low (Fig. 3D). In the other records discussed here, the alkenone concentration also decreased, which suggests low sea surface productivity in the Norwegian and Svalbard shelf areas (Fig. 4C). The low productivity in the region is also confirmed by high $\delta^{13}C$ and the low benthic foraminifera flux in Storfjordrenna (Fig. 3C) (Łącka et al., 2015b), as well as low benthic foraminifera flux further south, in Kveithola Trough (Groot et al., 2014). Two basic factors regulate primary productivity in the ocean: sunlight and nutrient availability. During the polar day, insolation is high, but light penetration throughout the water column can be limited by water turbidity. According to Łącka et al. (2015b), the sediment flux was low (approximately 0.019– 0.002 g cm^{-2} yr^{-1}; Fig. 3C) in Storfjordrenna during the mid-Holocene because of the reduced glaciers on Svalbard. Therefore, we suggest that the most important factor limiting primary productivity in the study area was nutrient availability. According to Behrenfeld et al. (2006), reduced nutrient flux into the upper oceans can be caused by enhanced thermal vertical stratification. The high SST in Storfjordrenna that prevailed approximately 6400 cal yr BP (Fig. 3A) most likely limited the surface cooling during the winter and consequently inhibited convective water mixing and the return of nutrients to the euphotic zone. Wollenburg et al. (2004) found that

484 productivity increased in the northern Barents Sea (at latitude 81°N) during the mid-Holocene.
485 The mid-Holocene productivity maximum (seen as maximum planktic and benthic foraminifera
486 abundances) was also noted by Ślubowska et al. (2005) in a sediment core obtained from the
487 northern Svalbard continental margin at 80°N. Thus, we suggest that the high productivity zone
488 at that time shifted northward to the region where Arctic pack ice appeared seasonally, causing
489 sea surface cooling in winter and inducing convective water mixing. Our suggestion is
490 supported by the northward and eastward shift of the ice edge and phytoplankton blooms in the
491 modern Barents Sea observed over the last 17 years (Oziel et al., 2017).

492 An alternative explanation of the low primary productivity in Storfjordrenna could be the
493 earlier light signal in the spring in the ice-free water and the earlier appearance of
494 mesozooplanktonic organisms in the sea surface. According to Zajączkowski et al. (2010), in
495 the ice-free Adventfjorden (western Spitsbergen), the open-water spring period enhanced
496 primary productivity. However, the majority of the particulate organic matter was then
497 consumed by zooplankton, and the organic matter sedimentation was much lower in this period
498 than in the ice-covered years. Additional investigations are needed to verify these two scenarios.

499 **5.5. Late Holocene (3400-1300 cal yr BP)**

500 After 3400 cal yr BP, the SSTs in Storfjordrenna decreased and ranged from 10°C to
501 approximately 0°C (Fig. 3A). Total alkenone flux increased rapidly (Fig. 3D). Throughout the
502 entire late Holocene, further gradual surface water cooling occurred, reflecting increases in
503 alkenone flux. A similar alkenone signal pattern was detected in both the southwestern Barents
504 Sea (Risebrobakken et al., 2010) and the Norwegian Sea (Calvo et al., 2002) (Fig. 4A and Fig.
505 4C). In general, this cooling trend corresponded to further decreases in northern hemisphere
506 insolation (Fig. 4D; Berger and Loutre, 1991). We suggest that the cooler surface of
507 Storfjordrenna froze periodically at that time and produced brine, which launched convective

water mixing and increased nutrient resupply to the sea surface. Consequently, primary production was enhanced in the area, as is supported by other productivity proxies such as higher benthic foraminifera flux (Łącka et al., 2015b). Simultaneously, diminished surface water productivity was noted in the inner Storfjorden, stemming from dense, packed sea ice cover (Knies et al., 2017). South of Storfjordrenna, in the Kveithola Trough, $P_{III}IP_{25}$ was mainly absent throughout the late Holocene, reflecting the predominantly ice-free ocean conditions (Belt et al., 2015) (Fig. 4D). According to Risebrobakken and Berben (2018), the AF in Kveithola Trough was shifted towards inner part of the trough at that time. We suggest that the difference in the location of the AF was caused by other local environmental conditions.

Late Holocene near-bottom conditions in Storfjordrenna were characterized by variable oceanographic conditions and higher salinity and temperature gradients because of the proximity of the AF that resulted from the reduced inflow of AW (Łącka et al., 2015b). This finding is supported by our new data on SSTs and other alkenone records published by Calvo et al. (2002) and Martrat et al. (2003) (Fig. 4A). SSTs decreased (c. 1-2°C), and marine productivity increased. Moreover, an increased $\%C_{37:4}$ (Fig. 3A) indicates a greater contribution of ArW, suggesting continuous sea ice formation inducing the convective replenishing of nutrients from the bottom to the surface.

6. Summary and conclusions

Alkenone analyses in sediment core JM-09-020GC from Storfjordrenna were performed with the purpose of reconstructing SSTs, the relative influences of AW and ArW, the location of the AF, as well as the marine primary productivity in the western Barents Sea between approximately 13,950 cal yr BP and 1300 cal yr BP. The proposed sequence of climatic and oceanographic events in the time period studied are as follows:

The SSTs in Storfjordrenna during the B-A warming were comparable to modern SST values. They were probably the result of increased insolation and the reinvigoration of the AMOC. However, we argue that the constant delivery of turbid meltwater from the Svalbard glaciers caused a significant decrease in marine productivity, unlike the present day situation in the core site location.

At the onset of the YD (12,800 cal yr BP), Storfjordrenna was covered by perennial sea ice, causing light limitations in the surface water and a subsequent reduction in phytoplankton growth. At approximately 12,600 cal yr BP, Storfjordrenna was covered by cold surface water, which we proposed caused water column stratification and was essential for sea ice formation. Thus, a marked pycnocline could have isolated the cold sea surface from the heat stored in the AW below. After 12,500 cal yr BP, the surface conditions in Storfjordrenna gradually ameliorated, and AW appeared at the surface, leading to a transition from the long seasonal ice cover to sea ice edge conditions. Although the YD is regarded as a stadial period, the present study shows that heavy sea ice conditions prevailed in Storfjordrenna only at the onset of the YD. In the middle part of the YD, the oceanography of Storfjordrenna was modified by interactions between Arctic and Atlantic waters, causing SST variability.

The early Holocene in Storfjordrenna (11,700- 9200 cal yr BP) was characterized by a transition from an Arctic to an Atlantic domain. The alkenone records can be interpreted to show that at approximately 11,500 cal yr BP, the AF passed the study site and moved eastward. Early Holocene warming was driven by the increasing northern hemisphere insolation and final decay of the SBSIS, leading to a shift from ice-sheet proximal to ice-sheet distal conditions at the study site. The high SSTs between 6400 and 3400 cal yr BP maintained water stratification in winter as well as inhibited convective water mixing and the return of nutrients to the euphotic zone and/or enhanced organic matter consumption by zooplankton, due to earlier light signals in the ice-free Storfjordrenna. The high productivity zone at this time shifted from

Storfjordrenna to the northern edge of the Eurasian shelf, where Arctic pack ice enabled sea surface cooling in winter and induced convective water mixing. During late the Holocene (3400-1300 cal yr BP), low insolation facilitated sea ice formation and brine production, which launched convective water mixing and increased nutrient resupply to the sea surface, consequently enhancing the primary productivity in Storfjordrenna.

Based on past changes in Arctic oceanography, combined with observations in the modern Barents Sea (e.g., Oziel et al., 2017), we suggest that the increasing inflow of warm AW and the disappearance of pack ice on the Eurasian continental shelf may weaken convective water mixing during the polar night and may limit spring/summer primary production in the region.

Acknowledgments

We acknowledge the National Science Centre in Poland for its financial support through project no. 2016/21/B/ST10/02308 (alkenone analysis) and 2012/05/N/ST10/03696 (other analyses) and the Spanish research Ministry Maria de Maeztu award MDM-2015-0552. We also extend our thanks to the captain and crew of the R/V Jan Mayen and the cruise participants, in particular Steinar Iversen, for their help at sea. Eva Calvo and Belen Martrat are gratefully acknowledged for providing their alkenone data. We are also very grateful to Agnieszka Promińska for data processing. We acknowledge two anonymous reviewers for their constructive comments on the manuscript.

References

Aagaard, K., Foldvik, A., Hillman, S. R., 1987. The West Spitsbergen Current: disposition and water mass transformation. J. Geophys. Res.: Oceans 92(C4), 3778-3784.

Andreassen, I., Nöthig, E.-M., Wassmann, P., 1996. Vertical particle flux on the shelf off northern Spitsbergen, Norway. Mar. Ecol. Prog. Ser.137, 215-228.

579 Antoniades, D., Francus, P., Pienitz, R., St-Onge, G., Vincent, W.F., 2011. Holocene dynamics
580 of the Arctic's largest ice shelf. Proc. Natl. Acad. Sci. U S A 108, 18899-18904.

581 Årthun, M., Eldevik, T., Smedsrud, L.H., Skagseth, Ø., Ingvaldsen, R., 2012. Quantifying the
582 influence of Atlantic heat on Barents Sea ice variability and retreat. J. Clim. 25, 4736-4743.

583 Bakke, J., Lie, Ø., Heegaard, E., Dokken, T., Haug, G. H., Birks, H. H., Dulski, P., Nilsen, T.,
584 2009. Rapid oceanic and atmospheric changes during the Younger Dryas cold period. Nature
585 Geosci. 2(3), 202.

586 Bartels, M., Titschack, J., Fahl, K., Stein, R., Seidenkrantz, M.-S., Hillaire-Marcel, C., Hebbeln,
587 D., 2017. Atlantic Water advection vs. glacier dynamics in northern Spitsbergen since early
588 deglaciation. Clim. Past 13, 1717-1749.

589 Behrenfeld, M.J., O'Malley, R.T., Siegel, D.A., McClain, C.R., Sarmiento, J.L., Feldman, G.
590 C., ..., Boss, E.S., 2006.Climate-driven trends in contemporary ocean productivity. Nature 444,
591 752–755 .

592 Belt, S.T., Cabedo-Sanz, P., Smik, L., Navarro-Rodriguez, A., Berben, S.M., Knies, J., Husum,
593 K., 2015. Identification of paleo Arctic winter sea ice limits and the marginal ice zone:
594 optimised biomarker-based reconstructions of late Quaternary Arctic sea ice. Earth Planet. Sci.
595 Lett. 431, 127-139.

596 Bendle, J., Rosell-Melé, A., 2004. Distributions of U^{K}_{37}UK37 and $U^{K'}_{37}$UK37′ in the surface
597 waters and sediments of the Nordic Seas: Implications for paleoceanography. Geochem.
598 Geophys. Geosyst. 5(11), Q11013.

599 Bendle, J., Rosell-Melé, A., Ziveri, P., 2005. Variability of unusual distributions of alkenones
600 in the surface waters of the Nordic seas. Paleoceanography 20, PA2001.

601 Berben, S., Husum, K., Cabedo-Sanz, P., Belt, S.T., 2014. Holocene sub-centennial evolution
602 of Atlantic water inflow and sea ice distribution in the western Barents Sea. Clim. Past 10, 181-
603 198.

604 Berger, A., Loutre, M.-F., 1991. Insolation values for the climate of the last 10 million years.
605 Quat. Sci. Rev. 10, 297-317.

606 Boitsov, V.D., Karsakov, A.L., Trofimov, A.G., 2012. Atlantic water temperature and climate
607 in the Barents Sea, 2000–2009. ICES J. Mar. Sci. 69, 833-840.

608 Bolton, C.T., Lawrence, K.T., Gibbs, S.J., Wilson, P.A., Cleaveland, L.C., Herbert, T.D., 2010.
609 Glacial–interglacial productivity changes recorded by alkenones and microfossils in late
610 Pliocene eastern equatorial Pacific and Atlantic upwelling zones. Earth Planet. Sci. Lett. 295,
611 401-411.

612 Brassell, S., Eglinton, G., Marlowe, I., Pflaumann, U., Sarnthein, M., 1986. Molecular
613 stratigraphy: a new tool for climatic assessment. Nature 320, 129-133.

614 Cabedo-Sanz, P., Belt, S.T., Knies, J., Husum, K., 2013. Identification of contrasting seasonal
615 sea ice conditions during the Younger Dryas. Quat. Sci. Rev. 79, 74-86.

616 Calvo, E., Grimalt, J., Jansen, E., 2002. High resolution U_{37}^{K}U 37 K sea surface temperature
617 reconstruction in the Norwegian Sea during the Holocene. Quat. Sci. Rev. 21, 1385-1394.

618 Conte, M.H., Sicre, M.A., Rühlemann, C., Weber, J.C., Schulte, S., Schulz-Bull, D., Blanz, T.,
619 2006. Global temperature calibration of the alkenone unsaturation index ($U_{37}^{K'}$UK′ 37) in surface
620 waters and comparison with surface sediments. Geochem. Geophys. Geosyst. 7(2),
621 2006Q02005.

622 Dalpadado, P., Ingvaldsen, R.B., Stige, L.C., Bogstad, B., Knutsen, T., Ottersen, G., Ellertsen,
623 B., 2012. Climate effects on Barents Sea ecosystem dynamics. ICES J. Mar. Sci. 69, 1303-
624 1316.

625 Dalpadado, P., Arrigo, K.R., Hjøllo, S.S., Rey, F., Ingvaldsen, R. B., Sperfeld, E., ..., Ottersen,
626 G., 2014. Productivity in the Barents Sea-response to recent climate variability. PloS one 9(5),
627 e95273.

628 Darby, D.A., Polyak, L., Bauch, H.A., 2006. Past glacial and interglacial conditions in the
629 Arctic Ocean and marginal seas–a review. Prog. Oceanogr. 71, 129-144.

630 Ding, Q., Schweiger, A., L'Heureux, M., Battisti, D.S., Po-Chedley, S., Johnson, N.C.,
631 Blanchard-Wrigglesworth, E., Harnos, K., Zhang, Q., Eastman, R., 2017. Influence of high-
632 latitude atmospheric circulation changes on summertime Arctic sea ice. Nat. Clim. Change
633 7,289–295.

634 Duplessy, J. C., Cortijo, E., Ivanova, E., Khusid, T., Labeyrie, L., Levitan, M., Murdmaa, I.,
635 and Paterne, M., 2005. Paleoceanography of the Barents Sea during the Holocene.
636 Paleoceanography 20, PA4004.

637 Fer, I., Skogseth, R., Haugan, P.M., Jaccard, P., 2003. Observations of the Storfjorden
638 overflow. Deep-Sea Res. Part I Oceanogr.50, 1283-1303.

639 Forwick, M., Vorren, T. O., 2009. LateWeichselian and Holocene sedimentary environments
640 and ice rafting in Isfjorden, Spitsbergen. Palaeogeogr. Palaeoclimatol. Palaeoecol. 280, 258–
641 274.

642 Gammelsrød, T., Leikvin, Ø., Lien, V., Budgell, W.P., Loeng, H., Maslowski, W., 2009. Mass
643 and heat transports in the NE Barents Sea: Observations and models. J. Mar. Syst. 75, 56-69.

644 Groot, D.E., Aagaard-Sørensen, S., and Husum, K., 2014. Reconstruction of Atlantic water
645 variability during the Holocene in the western Barents Sea. Clim. Past 10(1), 51-62.

646 Haarpaintner, J., Gascard, J.-C., Haugan, P.M., 2001. Ice production and brine formation in
647 Storfjorden, Svalbard. J. Geophys. Res. 106, 013.

648 Hald, M., Andersson, C., Ebbesen, H., Jansen, E., Klitgaard-Kristensen, D., Risebrobakken, B.,
649 Salomonsen, G.R., Sarnthein, M., Sejrup, H.P., Telford, R.J., 2007. Variations in temperature
650 and extent of Atlantic Water in the northern North Atlantic during the Holocene. Quat. Sci.
651 Rev. 26, 3423-3440.

652 Harada, N., Ahagon, N., Sakamoto, T., Uchida, M., Ikehara, M., Shibata, Y., 2006. Rapid
653 fluctuation of alkenone temperature in the southwestern Okhotsk Sea during the past 120 ky.
654 Glob. Planet. Change 53, 29-46.

655 Hendricks, S., Gerland, S., Smedsrud, L., Haas, C., Pfaffhuber, A., Nilsen, F., 2011. Sea-ice
656 thickness variability in Storfjorden, Svalbard. Ann. Glaciol. 52, 61-68.

657 Herbert, T., 2001. Review of alkenone calibrations (culture, water column, and sediments).
658 Geochem. Geophys. Geosyst.2, 2000GC000055.

659 Hoefs, M.J., Versteegh, G.J., Rijpstra, W.I.C., de Leeuw, J.W., Damsté, J.S.S., 1998.
660 Postdepositional oxic degradation of alkenones: Implications for the measurement of palaeo
661 sea surface temperatures. Paleoceanography 13(1), 42-49.

662 Hopkins, T.S., 1991. The GIN Sea: A synthesis of its physical oceanography and literature
663 review, 1972–1985. Earth Sci. Rev. 30, 175–318.

664 Hughes, A.L., Gyllencreutz, R., Lohne, Ø.S., Mangerud, J., Svendsen, J.I., 2016. The last
665 Eurasian ice sheets–a chronological database and time-slice reconstruction, DATED-1. Boreas
666 45, 1-45.

667 Ivanova, E., Murdmaa, I., de Vernal, A., Risebrobakken, B., Peyve, A., Brice, C., Seitkalieva,
668 E., Pisarev, S., 2019. Postglacial paleoceanography and paleoenvironments in the northwestern
669 Barents Sea. Quaternary Research, 1-20.

670 Kara, A.B., Wallcraft, A.J., Hurlburt, H.E., 2005. Sea surface temperature sensitivity to water
671 turbidity from simulations of the turbid Black Sea using HYCOM. J. Phys. Oceanogr. 35(1),
672 33-54.

673 Knies, J., Pathirana, I., Cabedo-Sanz, P., Banica, A., Fabian, K., Rasmussen, T.L., Forwick, M.,
674 Belt, S.T., 2017. Sea-ice dynamics in an Arctic coastal polynya during the past 6500 years.
675 Arktos 3, 1.

676 Knudsen, K.L., Eiríksson, J., Jansen, E., Jiang, H., Rytter, F., Gudmundsdóttir, E.R., 2004.
677 Palaeoceanographic changes off North Iceland through the last 1200 years: foraminifera, stable
678 isotopes, diatoms and ice rafted debris. Quat. Sci. Rev. 23, 2231-2246.

679 Kristensen, D.K., Rasmussen, T.L., Koç, N., 2013. Palaeoceanographic changes in the northern
680 Barents Sea during the last 16 000 years–new constraints on the last deglaciation of the
681 Svalbard–Barents Sea Ice Sheet. Boreas 42, 798-813.

682 Kubiszyn, A., Piwosz, K., Wiktor Jr, J., Wiktor, J., 2014. The effect of inter-annual Atlantic
683 water inflow variability on the planktonic protist community structure in the West Spitsbergen
684 waters during the summer. J. Plankton Res. 36, 1190-1203.

685 Lewandowska, A.M., Boyce, D.G., Hofmann, M., Matthiessen, B., Sommer, U., Worm, B.,
686 2014. Effects of sea surface warming on marine plankton. Ecol. Lett. 17, 614-623.

687 Lind, S., Ingvaldsen, R.B., 2012. Variability and impacts of Atlantic Water entering the Barents
688 Sea from the north. Deep-Sea Res. Part I Oceanogr. 62, 70-88.

689 Lind, S., Ingvaldsen, R.B., Furevik, T., 2018. Arctic warming hotspot in the northern Barents
690 Sea linked to declining sea-ice import. Nat. Clim. Change 8, 634–639.

691 Loeng, H., 1991. Features of the physical oceanographic conditions of the Barents Sea. Polar
692 Res. 10, 5-18.

693 Łącka, M., Pawłowska, J., Zajączkowski, M., 2015a. New Methods in the Reconstruction of
694 Arctic Marine Palaeoenvironments, Impact of Climate Changes on Marine Environments.
695 Springer, pp. 127-148.

696 Łącka, M., Zajączkowski, M., Forwick, M., Szczuciński, W., 2015b. Late Weichselian and
697 Holocene palaeoceanography of Storfjordrenna, southern Svalbard. Clim. Past 11, 587-603.

698 Mangerud, J., Svendsen, J. I.,2018. The Holocene Thermal Maximum around Svalbard, Arctic
699 North Atlantic; molluscs show early and exceptional warmth. Holocene 28(1), 65-83.

700 Marlowe, I., Brassell, S., Eglinton, G., Green, J., 1984. Long chain unsaturated ketones and
701 esters in living algae and marine sediments. Org. Geochem. 6, 135-141.

702 Martrat, B., Grimalt, J.O., Villanueva, J., van Kreveld, S., Sarnthein, M., 2003. Climatic
703 dependence of the organic matter contributions in the north eastern Norwegian Sea over the last
704 15,000 years. Org. Geochem. 34, 1057-1070.

705 Müller, J., Werner, K., Stein, R., Fahl, K., Moros, M., Jansen, E., 2012. Holocene cooling
706 culminates in sea ice oscillations in Fram Strait. Quat. Sci. Rev. 47, 1-14.

Müller, P.J., Kirst, G., Ruhland, G., Von Storch, I., Rosell-Melé, A., 1998. Calibration of the alkenone paleotemperature index $U^{K'}_{37}$U 37 K′ based on core-tops from the eastern South Atlantic and the global ocean (60° N-60° S). Geochim. Cosmochim. Acta 62, 1757-1772.

Müller, Peter J; Fischer, Gerhard, 2004. C_{37}-Alkenones as Paleotemperature Tool: Fundamentals Based on Sediment Traps and Surface Sediments from the South Atlantic Ocean. In: Wefer, G; Mulitza, S & Ratmeyer, V (eds.), The South Atlantic in the Late Quaternary: Reconstruction of Material Budgets and Current Systems, Springer, Berlin, Heidelberg, New York, 167-193.

Nilsen, F., Cottier, F., Skogseth, R., Mattsson, S., 2008. Fjord–shelf exchanges controlled by ice and brine production: the interannual variation of Atlantic Water in Isfjorden, Svalbard. Cont. Shelf Res. 28, 1838-1853.

Onarheim, I.H., Eldevik, T., Årthun, M., Ingvaldsen, R.B., Smedsrud, L.H., 2015. Skillful prediction of Barents Sea ice cover. Geophys. Res. Lett. 42, 5364-5371.

Oziel, L., Neukermans, G., Ardyna, M., Lancelot, C., Tison, J.L., Wassmann, P., Sirven, J., Ruiz-Pino, D., Gascard, J.C., 2017. Role for Atlantic inflows and sea ice loss on shifting phytoplankton blooms in the Barents Sea. J. Geophys. Res.: Oceans 122, 5121-5139.

Oziel, L., Sirven, J., Gascard, J.-C., 2016. The Barents Sea frontal zones and water masses variability (1980–2011). Ocean Sci. 12, 169-184.

Pathirana, I., Knies, J., Felix, M., Mann, U., 2014. Towards an improved organic carbon budget for the western Barents Sea shelf. Clim. Past 10, 569-587.

Pawłowska, J., Zajączkowski, M., Łącka, M., Lejzerowicz, F., Esling, P., Pawlowski, J., 2016. Palaeoceanographic changes in Hornsund Fjord (Spitsbergen, Svalbard) over the last millennium: new insights from ancient DNA. Clim. Past 12, 1459-1472.

730 Pearce, C., Seidenkrantz, M.-S., Kuijpers, A., Massé, G., Reynisson, N.F., Kristiansen, S.M.,
731 2013. Ocean lead at the termination of the Younger Dryas cold spell. Nat. Commun. 4, 1664.

732 Pfirman, S., Bauch, D., Gammelsrød, T., 1994. The northern Barents Sea: water mass
733 distribution and modification. AGU, American Geophysical Union.

734 Piwosz, K., Walkusz, W., Hapter, R., Wieczorek, P., Hop, H., Wiktor, J., 2009. Comparison of
735 productivity and phytoplankton in a warm (Kongsfjorden) and a cold (Hornsund) Spitsbergen
736 fjord in mid-summer 2002. Polar Biol. 32, 549-559.

737 Polyak, L., Alley, R.B., Andrews, J.T., Brigham-Grette, J., Cronin, T.M., Darby, D.A., Dyke,
738 A.S., Fitzpatrick, J.J., Funder, S., Holland, M., 2010. History of sea ice in the Arctic. Quat. Sci.
739 Rev. 29, 1757-1778.

740 Polyakov, I.V., Pnyushkov, A.V., Alkire, M.B., Ashik, I.M., Baumann, T.M., Carmack, E.C.,
741 Goszczko, I., Guthrie, J., Ivanov, V.V., Kanzow, T., 2017. Greater role for Atlantic inflows on
742 sea-ice loss in the Eurasian Basin of the Arctic Ocean. Science 356(6335), 285-291.

743 Rasmussen, T.L., Thomsen, E., 2014. Brine formation in relation to climate changes and ice
744 retreat during the last 15,000 years in Storfjorden, Svalbard, 76–78° N. Paleoceanography 29,
745 911-929.

746 Rasmussen, T.L., Thomsen, E., Nielsen, T., Wastegård, S., 2011. Atlantic surface water inflow
747 to the Nordic seas during the Pleistocene–Holocene transition (mid–late Younger Dryas and
748 Pre-Boreal periods, 12 450–10 000 a BP). J. Quat. Sci. 26, 723-733.

749 Rasmussen, T.L., Thomsen, E., Skirbekk, K., Ślubowska-Woldengen, M., Kristensen, D.K.,
750 Koç, N., 2014. Spatial and temporal distribution of Holocene temperature maxima in the
751 northern Nordic seas: interplay of Atlantic-, Arctic-and polar water masses. Quat. Sci. Rev. 92,
752 280-291.

753 Rasmussen, T.L., Thomsen, E., Ślubowska, M.A., Jessen, S., Solheim, A., Koç, N., 2007.
754 Paleoceanographic evolution of the SW Svalbard margin (76° N) since 20,000 14C yr BP. Quat.
755 Res. 67, 100-114.

756 Risebrobakken, B., Dokken, T., Smedsrud, L.H., Andersson, C., Jansen, E., Moros, M.,
757 Ivanova, E.V., 2011. Early Holocene temperature variability in the Nordic Seas: The role of
758 oceanic heat advection versus changes in orbital forcing. Paleoceanography 26, PA4206.

759 Risebrobakken, B., Moros, M., Ivanova, E.V., Chistyakova, N., Rosenberg, R., 2010. Climate
760 and oceanographic variability in the SW Barents Sea during the Holocene. Holocene20(4), 609-
761 621.

762 Risebrobakken, B., Berben, S.M.P., 2018. Early Holocene establishment of the Barents Sea
763 Arctic front. Front. Earth Sci., 6, 166.

764 Ritz, S.P., Stocker, T.F., Grimalt, J.O., Menviel, L., Timmermann, A., 2013. Estimated strength
765 of the Atlantic overturning circulation during the last deglaciation. Nat. Geosci. 6, 208-212.

766 Rosell-Melé, A., Carter, J., Eglinton, G., 1994. Distributions of long-chain alkenones and alkyl
767 alkenoates in marine surface sediments from the North East Atlantic. Org. Geochem. 22, 501-
768 509.

769 Rosell-Melé, A., Prahl, F.G., 2013. Seasonality of $U^{K'}_{37}$UK′ 37 temperature estimates as inferred
770 from sediment trap data. Quat. Sci. Rev. 72, 128-136.

771 Rosell-Mele, A., Weinelt, M., Sarnthein, M., Koc, N., Jansen, E., 1998. Variability of the Arctic
772 front during the last climatic cycle: application of a novel molecular proxy. Terra Nova Oxford
773 10, 86-89.

774 Rosell-Melé, A., 1998. Interhemispheric appraisal of the value of alkenone indices as
775 temperature and salinity proxies in high-latitude locations. Paleoceanography 13(6), 694-703.

776 Rudels, B., Korhonen, M., Schauer, U., Pisarev, S., Rabe, B., Wisotzki, A., 2015. Circulation
777 and transformation of Atlantic water in the Eurasian Basin and the contribution of the Fram
778 Strait inflow branch to the Arctic Ocean heat budget. Prog. Oceanogr. 132, 128-152.

779 Rueda, G., 2013. Reconstructing climate variability in the North Atlantic during the late
780 Holocene: an integrated biomarker approach The Autonomous University of Barcelona. The
781 Autonomous University of Barcelona, Barcelona, pp. 179.

782 Salvigsen, O., 2002. Radiocarbon-dated *Mytilus edulis* and *Modiolus modiolus* from northern
783 Svalbard: climatic implications. Norsk Geografisk Tidsskrift-Norwegian J. Geog. 56, 56-61.

784 Schauer, U., Rudels, B., Fer, I., Haugan, P., Skogseth, R., Björk, G., Winsor, P., 2003. Return
785 of deep shelf/slope convection in the Western Barents Sea, Seventh Conference on Polar
786 Meteorology and Oceanography and Joint Symposium on High-Latitude Climate Variations,
787 The American Meteorological Society.

788 Serreze, M.C., Barry, R.G., 2011. Processes and impacts of Arctic amplification: A research
789 synthesis. Glob. Planet. Change 77, 85-96.

790 Skogseth, R., Haugan, P., Haarpaintner, J., 2004. Ice and brine production in Storfjorden from
791 four winters of satellite and in situ observations and modeling. J. Geophys. Res.: Oceans 109,
792 C10008.

793 Slagstad, D., Ellingsen, I., Wassmann, P., 2011. Evaluating primary and secondary production
794 in an Arctic Ocean void of summer sea ice: an experimental simulation approach. Prog.
795 Oceanogr. 90, 117-131.

796 Smedsrud, L.H., Esau, I., Ingvaldsen, R.B., Eldevik, T., Haugan, P.M., Li, C., Lien, V.S., Olsen,
797 A., Omar, A.M., Otterå, O.H., 2013. The role of the Barents Sea in the Arctic climate system.
798 Rev. Geophys. 51, 415-449.

799 Smith, W.O., Sakshaug, E., 1990. Polar phytoplankton, in: Smith, W.O. (Eds.), Polar
800 oceanography, Part B: Chemistry, Biology and Geology. Academic Press, New York, pp. 447–
801 525.

802 Ślubowska, M.A., Koç, N., Rasmussen, T.L., Klitgaard-Kristensen, D., 2005. Changes in the
803 flow of Atlantic water into the Arctic Ocean since the last deglaciation: evidence from the
804 northern Svalbard continental margin, 80° N. Paleoceanography 20(4), PA4014.

805 Ślubowska-Woldengen, M., Koç, N., Rasmussen, T.L., Klitgaard-Kristensen, D., Hald, M.,
806 Jennings, A.E., 2008. Time-slice reconstructions of ocean circulation changes on the
807 continental shelf in the Nordic and Barents Seas during the last 16,000 cal yr BP. Quat. Sci.
808 Rev. 27, 1476-1492.

809 Ślubowska-Woldengen, M., Rasmussen, T.L., Koc, N., Klitgaard-Kristensen, D., Nilsen, F.,
810 Solheim, A., 2007. Advection of Atlantic Water to the western and northern Svalbard shelf
811 since 17,500 cal yr BP. Quat. Sci. Rev. 26, 463-478.

812 Thorarinsdóttir, G.G., Gunnarsson, K., 2003. Reproductive cycles of *Mytilus edulis* L. on the
813 west and east coasts of Iceland. Polar Res. 22, 217-223.

814 Trudnowska, E., Gluchowska, M., Beszczynska-Möller, A., Blachowiak-Samolyk, K.,
815 Kwasniewski, S., 2016. Plankton patchiness in the Polar Front region of the West Spitsbergen
816 Shelf. Mar. Ecol. Prog. Ser. 560, 1-18.

817 Volkman, J.K., Eglinton, G., Corner, E.D., Forsberg, T., 1980. Long-chain alkenes and
818 alkenones in the marine coccolithophorid *Emiliania huxleyi*. Phytochem. 19, 2619-2622.

Walczowski, W., 2013. Frontal structures in the West Spitsbergen Current margins. Ocean Sci. 9(6), 957–975.

Wollenburg, J.E., Knies, J., Mackensen, A., 2004. High-resolution paleoproductivity fluctuations during the past 24 kyr as indicated by benthic foraminifera in the marginal Arctic Ocean. Palaeogeogr. Palaeoclimatol. Palaeoecol. 204, 209-238.

Yang, X.-Y., Yuan, X., Ting, M., 2016. Dynamical link between the Barents–Kara sea ice and the Arctic Oscillation. J. Clim. 29, 5103-5122.

Zajączkowski, M., 2008. Sediment supply and fluxes in glacial and outwash fjords, Kongsfjorden and Adventfjorden, Svalbard. Polish Polar Res. 29, 59-72.

Zajączkowski, M., Nygård, H., Hegseth, E. N., Berge, J., 2010. Vertical flux of particulate matter in an Arctic fjord: the case of lack of the sea-ice cover in Adventfjorden 2006–2007. Polar Biol. 33(2), 223-239.